Acceleration Statistics of Neutrally Buoyant Spherical Particles in Intense Turbulence

Rachel D. Brown,[1] Z. Warhaft,[2] and Greg A. Voth[1]

[1]*Department of Physics, Wesleyan University, Middletown, Connecticut 06459, USA**

[2]*Sibley School of Mechanical and Aerospace Engineering, Cornell University, Ithaca, New York 14853, USA*

(Received 7 April 2009; published 5 November 2009)

We measure acceleration statistics of neutrally buoyant spherical particles with a diameter $0.4 < d/\eta < 27$ in intense turbulence ($400 < R_\lambda < 815$). High speed cameras image polystyrene tracer particles in a flow between counterrotating disks. The measurements of acceleration variance $\langle a^2 \rangle$ clearly resolve the transition from the tracer like behavior of small particles to the much smaller accelerations of large particles. Two models of this transition from small to large particle behavior are critically examined. For $d > 5\eta$, $\langle a^2 \rangle$ decreases with the diameter as $d^{-2/3}$, in agreement with inertial range scaling arguments. Consistent with earlier work, we find that the scaled acceleration probability density function shows very little dependence on particle size.

DOI: 10.1103/PhysRevLett.103.194501 PACS numbers: 47.27.Jv, 47.55.Kf

The motion of particles in turbulent fluid flows is a challenging multiscale problem that plays a central role in many areas of geophysics and engineering [1]. The parameter space for particle motion in turbulence contains a wide range of possibilities spanning both particle size and particle density. The most intensely studied region of this parameter space has been small particles with a density larger than the fluid [2,3], a problem relevant to many natural systems including water droplets in clouds and sedimentation. Significant study has also addressed small particles with positive buoyancy, such as air bubbles in water [4,5]. As long as the particles are small compared with the smallest scale of the turbulent motion, the particles can be modeled as points interacting with the fluid through a drag law [6,7]. The typical smallest scale is the Kolmogorov scale $\eta = \nu^{3/4}/\epsilon^{1/4}$ where ν is the kinematic viscosity of the fluid and ϵ is the energy dissipation rate.

Particles that are larger than η present profound analytical and computational difficulties. Because of the existence of the particle boundary layer, there are no analytical solutions of the equations of motion. Numerical simulations that resolve the particle boundary layer remain limited to extremely low Reynolds numbers despite significant progress in algorithms [8,9]. Effective equations of motion of large particles have been proposed that utilize phenomenological Faxén corrections to simulate the trajectories of large particles in turbulence [10]. Measurements are vital in order to evaluate these models and determine the range of particle sizes over which widely used point particle models are applicable. They are also of considerable practical importance since many marine organisms and tracer particles used in fluid experiments are large neutrally buoyant particles in a turbulent environment.

Here we present experimental measurements of the acceleration of neutrally buoyant particles at large Reynolds numbers for particle sizes that range from dissipative scales ($d = 0.4\eta$) into the inertial range ($d = 27\eta$). These measurements are the first to clearly resolve the transition from tracer particle to large particle behavior and allow a stringent test of various models that have been proposed to quantify the accelerations of large particles.

Two previous experiments have addressed this problem. Voth *et al.* [11] measured size dependence of particle accelerations in order to confirm tracer particle behavior. They suggested that the accelerations of these large particles might be modeled by terminating the cascade at the particle diameter d. The particle acceleration then scales with the fluid acceleration at the scale of the particle diameter, which implies $\langle a^2_{\text{particle}} \rangle \propto d^{-2/3}$ in the Kolmogorov inertial range. Qureshi *et al.* [12] measured accelerations of neutrally buoyant helium bubbles in a wind tunnel. Their particles ranged from 7η to $25\eta = 0.1L$ which at their relatively low Reynolds number ($R_\lambda = 160$), spans from the dissipation scales to the injection scales, but they are unable to observe the transition from dissipation to inertial range. They highlight the fact that the particle acceleration variance can be connected to the pressure structure function evaluated at the diameter of the particle, $\langle a^2_{\text{particle}} \rangle \propto \langle \Delta P^2(d) \rangle / d^2$ which gives the same $d^{-2/3}$ scaling in the inertial range for pressure structure functions that have $r^{4/3}$ inertial range scaling.

Lagrangian particle tracking measurements were carried out in the von Kármán flow between counterrotating disks described in [11]. The relevant parameters of the flow, including R_λ and the Kolmogorov microscales, are shown in Table I. Three Phantom v7 cameras (20 000 fps at 256 × 256 pixels) were arranged in the central horizontal plane and focused on a 1 cm^3 region at the center of the flow. A frequency-doubled, pulsed Nd:YAG laser with 50 W average power was used for illumination. Two beams were required to allow for forward scattering in all three cameras. Vertical polarization minimizes secondary reflections from the particles [13].

TABLE I. Table of flow parameters: f, frequency of the rotating disk; ν, kinematic viscosity of the fluid; $R_\lambda = (15\tilde{u}L/\nu)^{1/2}$, Taylor Reynolds number; $\tilde{u}$, rms velocity of the flow; $L = \tilde{u}^3/\epsilon$, energy input length scale; $\eta = (\nu^3/\epsilon)^{1/4}$, Kolmogorov length scale; $\tau_\eta = (\nu/\epsilon)^{1/2}$, Kolmogorov time scale; N_f, number of frames in each Kolmogorov time; V_i, the imaging volume; and Δx, the distance in the flow corresponding to one pixel.

f Hz	ν m^2/s	R_λ	$\tilde{u}$ m/s	L mm	ϵ m^2/s^3	η μm	τ_η ms	N_f Frames/τ_η	V_i η^3	x μm/pixel
5.25	1.00	813	0.62	71	3.41	23.3	0.54	11	430^3	41.1
5.25	1.29	717	0.62	71	3.41	28.2	0.62	12	355^3	41.1
1.6	1.00	449	0.19	71	0.10	56.9	3.23	64	175^3	41.1
1.6	1.29	396	0.19	71	0.10	68.7	3.66	73	145^3	41.1

All particles used were polystyrene spheres ($\rho = 1.05$ g/cm^3). Measurements were made with the flow seeded with both monodispersed particles (Duke Scientific) with known diameters ($d = 26$, 55, 134, 222, 300, 400 μm) and with polydispersed "grinding media" with diameters in the range 600–990 μm (Norstone, Inc.). We use a reflection pair method to determine the diameter of the large particles from the images of each trajectory. The central camera records two reflections from each particle in the imaging volume because of the two beams. For large particles ($d > 100$ μm) the two reflections can be resolved, allowing measurements of particle size in every frame with an uncertainty of 20 μm. Excluding particles whose diameter changes over time minimizes error due to the small fraction of nonspherical particles in the grinding media.

An 8% NaCl solution by mass ($\nu = 1.29 \times 10^6$ m^2/s, $\rho = 1.048$ g/cm^3) is used in order to density match particles with diameters greater than 100 μm, but deionized water is used for 26 and 55 μm particles. The effect of a 5% density mismatch on particle accelerations is nearly negligible for all our particle sizes [11]; but keeping the large particles suspended requires careful density matching.

We use the data acquisition system described in [14]. Images are acquired in 1 s sequences, which take 3–5 min to download. Particle positions extracted from the images are stored and later tracked. For each particle size, we obtain on average 65×10^6 particle positions from 40–500 sequences. Accelerations are determined by quadratic fits to the particle trajectories. Figure 1 shows the measured acceleration variance for one data set as a function of fit time. For the highly intermittent accelerations of particles in turbulence, it is difficult to obtain fits that are not affected either by measurement errors or by smoothing of the trajectories. We use an established method [11] to extrapolate back to zero fit time in order to determine the acceleration variance.

All results reported in this Letter are from analysis of two dimensional trajectories. With three cameras, it is possible to determine 3D trajectories. However, we encountered difficulties with stereomatching from images of particles that fill a large fraction of the field of view and so the 3D tracks are extremely fractured. As a result, we find much better statistical convergence for the 2D trajectories. We focus on the axial component of acceleration (parallel to the axis of rotation of the disks in our flow). The transverse component shows similar results with larger measurement uncertainties. For fluid particles, the transverse acceleration variance in this flow is 10% to 20% larger than the axial variance [11].

Figure 2(a) shows acceleration variance measurements as a function of particle diameter. The acceleration is normalized by Kolmogorov variables to give a_0. For small particle diameters ($d/\eta \leq 5$) the normalized acceleration variance is nearly constant. At larger diameters the normalized acceleration variance falls off implying that these large particles do not simply trace the flow. There is no detectable dependence on Reynolds number. However, at the lower Reynolds number, the largest particles studied are only 10.9η. For fluid particles, a_0 is found to vary by less than 17% over the Reynolds number range we study [11]. Data are presented for two methods of determining particle positions. The first method treats each reflection observed in an image as a particle. This method works well for monodispersed particles, $d \leq 400$ μm, and we can use data from all three cameras to improve statistical convergence. The second method was developed to determine the size of polydisperse particles from the images. Here we use only the central camera, and require two reflections to be

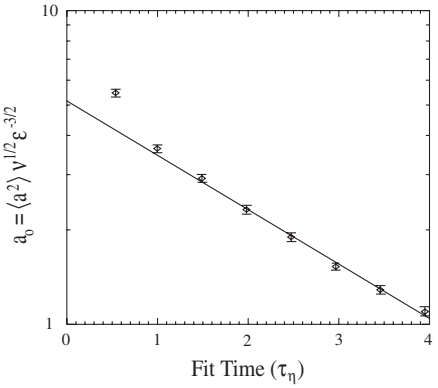

FIG. 1. An example extrapolation back to zero fit time. Acceleration variance for single reflection measurements of the 300 μm ($d/\eta = 10.64$) particles taken at $R_\lambda = 717$ are plotted along with the statistical errors.

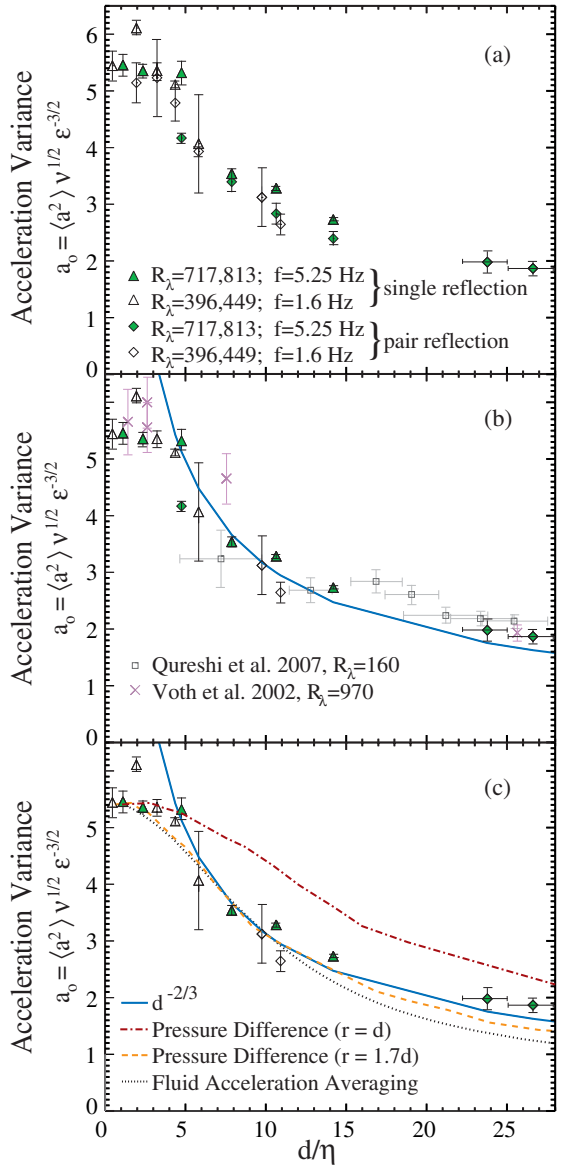

FIG. 2 (color online). (a) Acceleration variance as a function of particle diameter. Unfilled symbols represent data taken at the lower disk frequency ($R_\lambda = 396, 449$). Filled symbols represent data taken at the higher disk frequency ($R_\lambda = 717, 813$). Triangles are single reflection measurements. Diamonds are reflection pair measurements. (b) X's are measurements from [11]. Gray squares from [12]. The solid curve is the $d^{-2/3}$ inertial range scaling. Pair measurements are not shown for data sets where single reflection measurements are available. (c) Symbols are the same as in (a). The solid curve is the $d^{-2/3}$ inertial range scaling. The dashed curves show the predictions of the pressure difference model. The dot-dashed line uses a separation equal to the particle diameter. The dashed line uses the separation which best fits our data ($1.7d$). The dotted curve is the prediction of the fluid acceleration averaging model.

observed that move parallel to each other. This analysis can be done for particles with diameter $d \geq 134$ μm. Data points are plotted for both of these methods to show that no systematic error is introduced when we use the reflection pair method. Error bars in Fig. 2 represent statistical uncertainties. A 10% uncertainty in the energy dissipation rate measurement produces a systematic error of 15% in a_0 and 2.5% in η [13] which are not shown. This does not affect the model comparisons below because they use data measured in this same flow. There is also a small systematic error associated with the extrapolation [11]. Figure 2(b) includes data from two previous measurements of accelerations of large particles.

Figure 2(c) shows the measured acceleration variance compared with predictions from three models. The first of these models is the $d^{-2/3}$ scaling predicted for particles with diameters in the inertial range [11]. Our data show good agreement with the $d^{-2/3}$ scaling for $d > 5\eta$.

A second model is suggested by the connection between the particle acceleration variance and the pressure structure function [12]. In addition to showing $d^{-2/3}$ inertial range scaling, this pressure difference model can be extended to predict the acceleration variance for small particle diameters $d < \eta$ using the pressure structure function for separation distances in the dissipation range. In a previous experiment in the same apparatus, Xu *et al.* [15] measured the pressure structure function over the range $0.7\eta < r < 140\eta$. We use their data to create the prediction shown as a dot-dashed line in Fig. 2(c). When the separation at which the pressure difference is sampled is equal to the particle diameter, this model predicts larger accelerations than we measure at large particle sizes. However, this model is a good fit when we allow the separation to be an adjustable parameter and sample the pressure structure functions at $(1.7 \pm 0.3)d$. The mechanism which would cause the particle's acceleration to be determined by length scales larger than its diameter is unclear.

The third model assumes that the particle acceleration is equal to the spatial average of the fluid acceleration over the volume of a particle. This model closely matches the model used by Calzavarini *et al.* [10]. Their model differs by a drag term that contributes only 1% to the neutrally buoyant particle acceleration. In this fluid acceleration averaging model, the particle acceleration variance is given by

$$\langle a_{\text{particle}}{}^2 \rangle = \frac{1}{V^2} \int_v \int_{v'} \langle a_f(\mathbf{r}) a_f(\mathbf{r}') \rangle d^3\mathbf{r} d^3\mathbf{r}'. \quad (1)$$

Integrating and using the isotropic expression, $R_{ij} = R_{NN}\delta_{ij} + (R_{LL} - R_{NN}) r_i r_j / r^2$ for the acceleration correlation function yields

$$\frac{\langle a_{\text{particle}}{}^2 \rangle}{\langle a_f{}^2 \rangle} = \frac{8}{d^3} \int_0^{d/2} (2R_{NN}(r) + R_{LL}(r)) r^2 dr. \quad (2)$$

Xu *et al.* [15] have measured the acceleration correlation functions, $R_{LL}(r)$ and $R_{NN}(r)$, in the flow that we study. Integrating their measured functions in Eq. (2) produces the dotted curve shown in Fig. 2(c). This model gives a very good fit to our data both at small scales and in the transition to inertial range scaling without the use of any

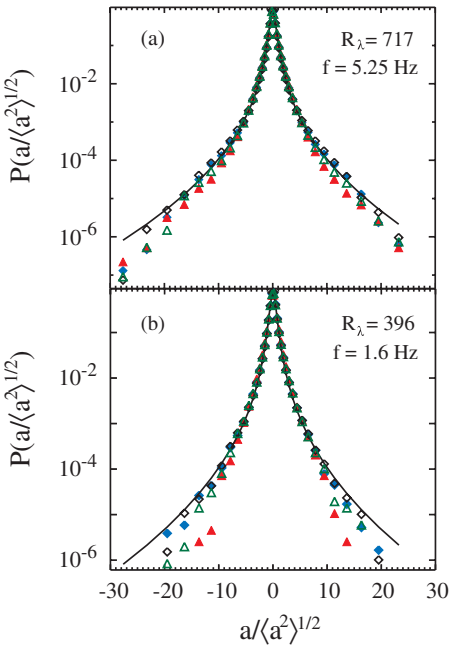

FIG. 3 (color online). Probability density functions of acceleration at Taylor Reynolds numbers (a) 717 and (b) 396. Particle sizes in d/η represented by each symbol are as follows: black unfilled diamonds, (a) 1.95 and (b) 4.75; blue filled diamonds, (a) 3.23 and (b) 7.87; green unfilled triangles, (a) 4.37 and (b) 10.64; and red filled triangles, (a) 5.82 and (b) 14.18.

free parameters, thus performing somewhat better than the pressure difference model. However, this third model predicts accelerations that are slightly too small for large particle sizes. It also does not display $d^{-2/3}$ scaling in the range of particle sizes we studied. The acceleration correlation functions do not show inertial range scaling until $d > 40\eta$ [15], and so inertial range scaling for this model is not expected in the range $d < 25\eta$ that we study. Although the data seems to match the $d^{-2/3}$ scaling quite well, the lack of scaling in the acceleration correlation functions suggests the possibility that the observed $d^{-2/3}$ scaling for small particles sizes is only approximate and that much larger particles sizes (along with high Reynolds numbers) are needed before rigorous $d^{-2/3}$ scaling will exist. Figure 3 shows the probability density function (PDF) of particle accelerations normalized by the standard deviation for particle sizes $d < 15\eta$. Within our measurement error, these PDFs agree with the form of the fluid acceleration PDF [16]. In the tails of the PDFs, the probability densities for large particles sizes may be slightly below the fluid particle PDF. This is more pronounced in the data from the large polydispersed particles (not shown). However, in looking carefully at our data we found errors due to particle finding, tracking, and nonspherical or stray particles that seem to affect the rare events by as much as any discrepancy with the fluid acceleration PDF, so we do not draw any conclusions from these slight differences. This particle size independence of the acceleration PDFs has been observed before [11,12,17] and remains puzzling.

These measurements of accelerations of spherical neutrally buoyant particles in intense turbulence clearly resolve the transition from the tracer regime to the large particle regime. The acceleration variance as a function of particle size show the best agreement yet measured with the inertial range $d^{-2/3}$ scaling. We present two models that capture the transition from tracer to large particle behavior. The success of these simple phenomenological models is perhaps surprising given the complex flow in the boundary layer around large particles in turbulence. We hope that more rigorously derived models and data at still larger particle sizes will become available in the future. The parameter space of this problem is vast, but these measurements seem to put our understanding of one region, large neutrally buoyant particles, on a solid foundation.

This work was supported by NSF Grants No. DMR-0547712 to Wesleyan University and No. NSF-0756501 to Cornell. We thank Eberhard Bodenschatz, Haitao Xu, Nick Ouellette, Mark Nelkin, Stephanie Neuscamman, and Sergey Gerashchenko.

*http://gvoth.web.wesleyan.edu/lab.htm

[1] F. Toschi and E. Bodenschatz, Annu. Rev. Fluid Mech. **41**, 375 (2009).
[2] K. D. Squires and J. K. Eaton, Phys. Fluids A **3**, 1169 (1991).
[3] S. Ayyalasomayajula, A. Gylfason, L. R. Collins, E. Bodenschatz, and Z. Warhaft, Phys. Rev. Lett. **97**, 144507 (2006).
[4] I. M. Mazzitelli and D. Lohse, New J. Phys. **6**, 203 (2004).
[5] R. Volk, E. Calzavarini, G. Verhille, D. Lohse, N. Mordant, J.-F. Pinton, and F. Toschi, Physica (Amsterdam) **237D**, 2084 (2008).
[6] J. Bec, L. Biferale, G. Boffetta, A. Celani, M. Cencini, A. Lanotte, S. Musacchio, and F. Toschi, J. Fluid Mech. **550**, 349 (2006).
[7] E. Calzavarini, M. Cencini, D. Lohse, and F. Toschi, Phys. Rev. Lett. **101**, 084504 (2008).
[8] A. T. Cate, J. J. Derksen, L. M. Portela, and H. E. A. V. D. Akker, J. Fluid Mech. **519**, 233 (2004).
[9] Z. Zhang and A. Prosperetti, J. Comput. Phys. **210**, 292 (2005).
[10] E. Calzavarini, R. Volk, M. Bourgoin, E. Leveque, J.-F. Pinton, and F. Toschi, arXiv:org:0811.4410v2.
[11] G. A. Voth, A. La Porta, A. M. Crawford, J. Alexander, and E. Bodenschatz, J. Fluid Mech. **469**, 121 (2002).
[12] N. M. Qureshi, M. Bourgoin, C. Baudet, A. Cartellier, and Y. Gagne, Phys. Rev. Lett. **99**, 184502 (2007).
[13] G. A. Voth, Ph.D. thesis, Cornell University, 2000.
[14] N. T. Ouellette, H. Xu, M. Bourgoin, and E. Bodenschatz, New J. Phys. **8**, 109 (2006).
[15] H. Xu, N. T. Ouellette, D. Vincenzi, and E. Bodenschatz, Phys. Rev. Lett. **99**, 204501 (2007).
[16] N. Mordant, A. M. Crawford, and E. Bodenschatz, Physica (Amsterdam) **193D**, 245 (2004).
[17] H. Xu and E. Bodenschatz, Physica (Amsterdam) **237D**, 2095 (2008).